Cell

Bombesin-like peptide recruits disinhibitory cortical circuits and enhances fear memories

Graphical abstract

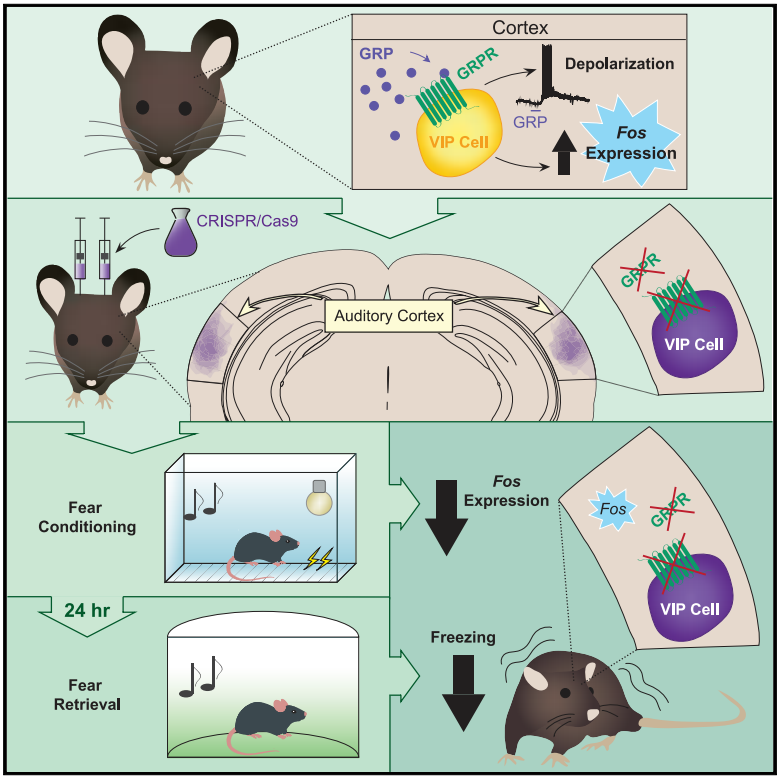

Highlights

- Gastrin-releasing peptide (GRP) receptors are expressed in cortical VIP cells
- GRP modulates cortical disinhibitory VIP cell activity and gene expression
- Cortical VIP cells activate to novel sounds and shocks during fear conditioning
- Ablation of GRP receptor in auditory cortex results in impaired fear memory

Authors

Sarah Melzer, Elena R. Newmark, Grace Or Mizuno, ..., James Levasseur, Lin Tian, Bernardo L. Sabatini

Correspondence

bsabatini@hms.harvard.edu

In brief

Critical function of neuropeptides in cortex-dependent behaviors is demonstrated by local and long-range sources of the neuropeptide, GRP, selectively recruiting disinhibitory cortical microcircuits in auditory cortex to regulate fear memories in mice.

Melzer et al., 2021, Cell *184*, 5622–5634
October 28, 2021
https://doi.org/10.1016/j.cell.2021.09.013

CellPress

CellPress

Cell

Article

Bombesin-like peptide recruits disinhibitory cortical circuits and enhances fear memories

Sarah Melzer,[1] Elena R. Newmark,[1] Grace Or Mizuno,[2] Minsuk Hyun,[1] Adrienne C. Philson,[1] Eleonora Quiroli,[1] Beatrice Righetti,[1] Malika R. Gregory,[1] Kee Wui Huang,[1] James Levasseur,[1] Lin Tian,[2] and Bernardo L. Sabatini[1,3,*]

[1]Department of Neurobiology, Howard Hughes Medical Institute, Harvard Medical School, 220 Longwood Avenue, Boston, MA 02115, USA

[2]Departments of Biochemistry and Molecular Medicine, School of Medicine, University of California, Davis, Davis, CA, USA

[3]Lead contact

*Correspondence: bsabatini@hms.harvard.edu

https://doi.org/10.1016/j.cell.2021.09.013

SUMMARY

Disinhibitory neurons throughout the mammalian cortex are powerful enhancers of circuit excitability and plasticity. The differential expression of neuropeptide receptors in disinhibitory, inhibitory, and excitatory neurons suggests that each circuit motif may be controlled by distinct neuropeptidergic systems. Here, we reveal that a bombesin-like neuropeptide, gastrin-releasing peptide (GRP), recruits disinhibitory cortical microcircuits through selective targeting and activation of vasoactive intestinal peptide (VIP)-expressing cells. Using a genetically encoded GRP sensor, optogenetic anterograde stimulation, and *trans*-synaptic tracing, we reveal that GRP regulates VIP cells most likely via extrasynaptic diffusion from several local and long-range sources. *In vivo* photometry and CRISPR-Cas9-mediated knockout of the GRP receptor (GRPR) in auditory cortex indicate that VIP cells are strongly recruited by novel sounds and aversive shocks, and GRP-GRPR signaling enhances auditory fear memories. Our data establish peptidergic recruitment of selective disinhibitory cortical microcircuits as a mechanism to regulate fear memories.

INTRODUCTION

Cortical circuits consist of multiple cell classes whose orchestrated activity is crucial for signal processing and plasticity. The post-synaptic specificity of afferent and intracortical inputs permits the temporally precise regulation of different cortical cell classes during behavior (Karnani et al., 2016; Pfeffer et al., 2013; Pi et al., 2013). For example, cortical inputs facilitate neuronal mismatch responses (Leinweber et al., 2017), suppress responses to predicted and unattended stimuli (Iurilli et al., 2012), or enhance sensory responses and plasticity (Fu et al., 2014, 2015; Lee et al., 2013; Zhang et al., 2014) by targeting mainly excitatory, inhibitory, or disinhibitory cortical neurons, respectively. Thus, cortical circuit motifs are regulatory control points that can be differentially activated to induce behaviorally relevant changes in cortical state.

The specificity of the expression of receptors for neuromodulators, signaling molecules that often act through slower extrasynaptic transmission, suggests that multiple channels of cortical neuromodulator-based communication exist that also regulate functionally relevant network activity (Marlin et al., 2015; Nakajima et al., 2014; Smith et al., 2019; Tasic et al., 2016). Nevertheless, most cortical neuropeptides have not been investigated with respect to their cellular and behavioral effects.

Within cortex, vasoactive-intestinal peptide (VIP)-expressing neurons, due to their synaptic targets, are well-positioned to control circuit excitability and plasticity (Adler et al., 2019; Batista-Brito et al., 2017; Fu et al., 2014, 2015; Karnani et al., 2016; Pfeffer et al., 2013; Pi et al., 2013). VIP cells express a diverse set of neuromodulator receptors (Smith et al., 2019; Tasic et al., 2016, 2018), making them likely targets of local and long-range neuromodulatory systems.

One neuromodulator with unknown function in most cortical brain areas is gastrin-releasing peptide (GRP), a bombesin-like peptide that binds to the G protein-coupled GRP receptor (GRPR) with high affinity and selectivity (Kroog et al., 1995). GRP release in different parts of the CNS mediates itch (Sun and Chen, 2007) and sighing (Li et al., 2016b) and has been implicated in fear memories (Mountney et al., 2006, 2008; Roesler et al., 2003).

Here, we identify GRPR as a regulator of VIP cell-dependent signaling and behavior. We demonstrate that GRPR is expressed nearly exclusively in VIP cells in many cortical regions. Endogenous GRPR signaling during fear conditioning induces immediate early gene (IEG) expression in VIP cells, consistent with a role for GRP in facilitating excitability. Furthermore, CRIPSR/Cas9-mediated and conditional knockout (KO) of GRPR in auditory cortex (ACx) diminishes fear memories in control but not GRP KO mice in a discriminatory auditory fear conditioning task (Letzkus et al., 2011) that engages VIP cells in a cue- and novelty-dependent manner. Our results thus highlight the importance of neuropeptidergic cell-type-specific communication channels in regulating functionally relevant cortical circuits.

RESULTS

Cortex-wide expression of GRP and its receptor

To identify candidate neuromodulator receptors for selective regulation of VIP cells, we analyzed gene expression in mouse visual cortex in two single-cell RNA sequencing (scRNA-seq) datasets (Tasic et al., 2016, 2018) and identified the gastrin-releasing peptide receptor (*Grpr*) (Figure S1A) as a candidate for VIP cell-specific peptidergic neuromodulation (as proposed previously, see Smith et al. [2019]). Fluorescent *in situ* hybridization (FISH) targeting the gene encoding its specific ligand, gastrin-releasing peptide (*Grp*), revealed mRNA expression in 28% ± 5% of glutamatergic cells across cortex (96% ± 0% of *Grp*$^+$ cells were *Slc17a6/7/8*$^+$ whereas only 3% ± 0% were *Gad1/2*) (Figures 1A–1C, 1E, 1F, S1B, and S1C). Furthermore, *Grpr* expression was detected in 81% ± 2% of *Vip*$^+$ cells, and 83% ± 3% of *Grpr*$^+$ cells expressed *Vip* (Figures 1D–1F and S1D). Similar numbers were found during early postnatal development (Figure S1E) suggesting preserved GRPR-mediated signaling throughout development and adulthood.

Because 19% of *Grpr*$^+$ cells were *Vip*-negative GABAergic neurons (Figure 1F), we examined whether *Grpr* is present in other major inhibitory cell types and detected *Sst* and *Pvalb* expression in a subset of *Grpr*$^+$ cells (Figure S1F). In contrast, in the adult mouse hippocampus, an area with comparably high levels of *Grpr*, expression was relatively evenly distributed among the three major GABAergic cell types (Figure S1G), suggesting that preferential VIP cell targeting by GRP is a brain area-dependent feature.

Several neuropeptidergic systems are evolutionarily conserved (Jékely et al., 2018), raising the question as to whether GRPR signaling follows similar principles in human cortex as in mouse. Indeed, FISH in the human visual cortex (BA17) showed that a large proportion of *GRPR*$^+$ cells expressed *VIP* and *GAD1*, but rarely *SST* and *PVALB* (Figures 1G–1I and S1H), suggesting that the neocortical GRP-GRPR signaling pathway is evolutionarily conserved between mouse and human. The large fraction of human *GRPR*$^+$ cells that lack *VIP* expression may represent a distinct GABAergic *VIP/SST/PVALB*-negative cell class or cells in which *VIP* mRNA levels are below detection threshold. Consistent with the former, scRNA-seq data show expression of *GRPR* in *LAMP1*$^+$ putative layer 1 neurons (Hodge et al., 2019) that are thought to have a disinhibitory function analogous to that of VIP cells (Letzkus et al., 2011).

Putative local and long-range sources of GRP

The patterns of expression of *Grp* suggest that it is expressed by cortico-cortical or cortico-thalamic neurons, both of which reside in L6 (Briggs and Usrey, 2011). To identify cortico-thalamic neurons, we injected cholera toxin B (CTB) into the auditory thalamus (Figures 2A and 2B). FISH revealed that 86% ± 4% of *Grp*$^+$ cells in L6 were retrogradely labeled with CTB (n = 958 *Grp*$^+$ cells in 4 hemispheres), and L6 *Grp*$^+$ neurons constitute a subpopulation of cortico-thalamic neurons (41% ± 10% out of 1,494 CTB$^+$ cells in 4 hemispheres) (Figure 2C). Similar results were obtained after injections into the motor thalamus (Figure S2A), establishing L6 cortico-thalamic neurons as a putative source of cortical GRP signaling.

We also detected strong *Grp* expression in several input areas of the ACx including the lateral amygdala (LA), contralateral ACx (clACx,) temporal association area (TeA), perirhinal cortex (Per), and auditory thalamic nuclei including the medial part of the medial geniculate nucleus (MGM) and the suprageniculate nucleus (SG), suggesting that these might be sources of cortical GRP. To examine this possibility, we injected CTB into the ACx (Figure 2D) and analyzed *Grp* expression by FISH (Figures 2E, S2B, and S2C). Indeed, the majority of CTB$^+$ cells in the LA and approximately half of the CTB$^+$ cells in the thalamus and in Per were *Grp*$^+$. Less coexpression occurred in the TeA and clACx. In each area, only a small population of *Grp*$^+$ cells were CTB$^+$ (Figure 2E), suggesting that a subset of *Grp*$^+$ cells are putative long-range sources of GRP in cortex.

Whereas fast synaptic neurotransmission typically occurs between specific subsets of directly connected neurons, extrasynaptic diffusion of neuropeptides may allow these neuromodulators to reach all cells in a target region. To test whether VIP cells receive synaptic inputs and peptidergic signals from overlapping or distinct subsets of neurons, we used pseudotyped rabies virus (RabV) transsynaptic retrograde labeling from ACx VIP cells (Figures 2F, 2G, S2D, and S2E). Only a small subpopulation of retrogradely labeled neurons expressed *Grp* in ACx and posterior portions of the auditory thalamus (Figures 2H, 2I, and S2F). Similar results were obtained after injections into M1 (Figures S2G and S2H), suggesting that VIP cells across multiple cortical areas receive GRP signals from a neuronal population that is largely distinct from that which provides direct synaptic input (Figure 2J).

To confirm these results, we optogenetically stimulated amygdalo-cortical projections, a majority of which are *Grp*$^+$ (Figure S2I), and examined evoked excitatory postsynaptic currents (EPSCs) in L2/3 VIP cells and neighboring pyramidal (Pyr) cells in the primary ACx using whole-cell recordings. Consistent with our retrograde labeling results, the majority of ACx cells did not receive direct synaptic inputs (Figure S2J). This was not due to a failure to efficiently activate axonal projections, since most VIP and Pyr cells recorded in L2/3 of the TeA within the same brain slices received strong synaptic inputs (Figure S2J).

Extrasynaptic GRP signaling requires that the peptide be stable and efficiently diffuse through extracellular space. To monitor GRP diffusion *in vivo*, we developed a genetically encoded GRP sensor (grpLight) based on a previously established platform (Patriarchi et al., 2018) (Figures S2K–S2M). GrpLight showed high specificity for GRP compared to other common neuropeptides and could detect nanomolar concentrations of GRP (Figures S2N–S2Q). *In vivo* photometric imaging of grpLight green fluorescence in the ACx following infusion of red fluorescently tagged GRP (TAMRA-GRP) into a distant cortical area revealed long-lasting increases minutes after the start of GRP infusion (Figures S2R–S2T). Our results show that GRP diffuses slowly and maintains biological activity for over an hour in intact brain tissue, suggesting that GRP is a long-acting peptide that reaches large neuronal populations through extrasynaptic diffusion.

GRP depolarizes and increases intracellular Ca^{2+} in cortical VIP cells

The cell-type specificity of *Grpr* expression suggests that VIP cells are the primary targets of modulation by GRP. Whole-cell

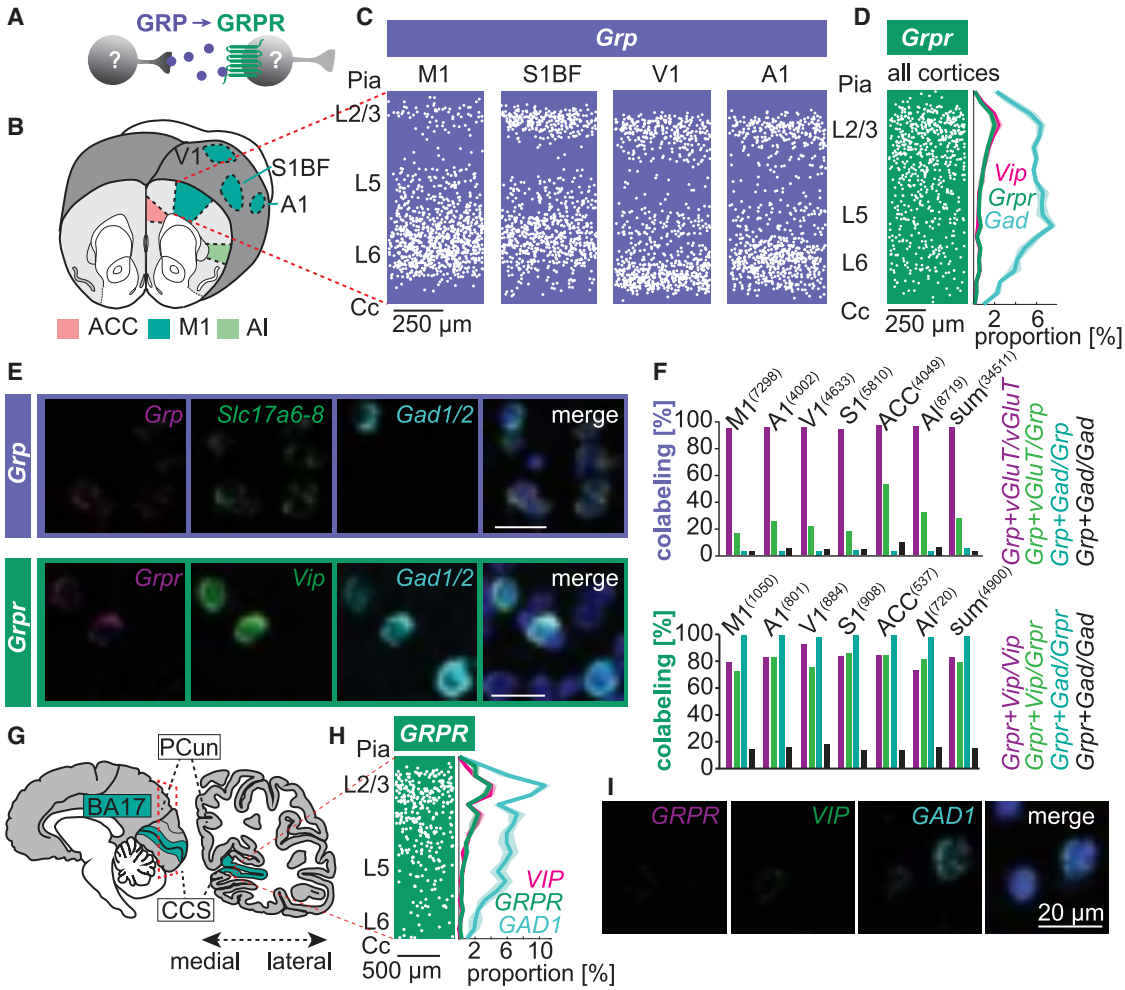

Figure 1. Cortex-wide, cell-type-specific expression of GRP and its receptor

(A) Schematic of GRP release and binding to GRP receptor (GRPR) in unidentified cell types.

(B) GRP and GRPR expression were analyzed in mice in the indicated areas. Abbreviations: M1, primary motor; A1, primary auditory; V1, primary visual; S1BF, primary somatosensory-barrel field; ACC, anterior cingulate; AI, anterior insular cortex.

(C) Locations of all identified *Grp*$^+$ cells in the indicated areas (n = 5 slices for S1BF, V1, A1, and 7 for M1). See also Figure S1.

(D) Locations of all identified *Grpr*$^+$ cells in indicated areas (n = 34 slices, 4,900 cells). Quantification of the proportions (mean ± SEM) of cells that are *Grpr*$^+$, *Vip*$^+$, or *Gad*$^+$ across cortical depth (20 bins).

(E) Representative confocal images of mouse cortex showing coexpression of *Grp* (top) and *Grpr* (bottom) with *Vip*, glutamatergic markers (*Slc17a6-8* encoding vGluT1-3) and GABAergic markers (*Gad1,2*). Scale bars, 20 µm.

(F) Quantification of coexpression of *Grp* (top) and *Grpr* (bottom) with indicated genes. Numbers of analyzed cells per area are indicated above bars (≥15 slices from 4–7 hemispheres per area).

(G) Schematic of human visual cortex (BA17) in which *GRPR* expression was analyzed using FISH.

(H) Left: locations of all identified *GRPR*$^+$ cells in 5 sections of human visual cortex. Right: quantification of the proportions (mean ± SEM) of cells that are *GRPR*$^+$, *VIP*$^+$, and *GAD1*$^+$ (n = 882 cells; 20 bins).

(I) Representative confocal image of a *GRPR*$^+$/*VIP*$^+$/*GAD1*$^+$ human cell.

See also Figure S1.

current-clamp recordings in ACx VIP cells (using *Vip*-EGFP mice) of male mice revealed that most VIP cells (7 out of 10) depolarize upon GRP bath application (300 nM for 2 min), occasionally resulting in long-lasting (>1 min) burst-like firing activity (3 out of 10 neurons) (Figures 3A, 3B, S3A, and S3B). Depolarization was concentration-dependent (Figure 3C) and strongly reduced by a GRPR antagonist (Figure S3B). Because the *Grpr* gene is on the X chromosome, we separately examined VIP cell responses in female mice and found a non-significantly larger depolarization compared to male mice (Figure S3C). Similar results were obtained in M1 (Figure S3E).

To confirm that the effects of GRP are largely VIP cell-specific, we obtained current-clamp recordings from SST, PVALB, and Pyr cells in the ACx (Figure 3D) and M1 (Figure S3F). GRP-evoked depolarizations in all three cell types were significantly smaller than in VIP cells (Figures 3E and S3G). No significant

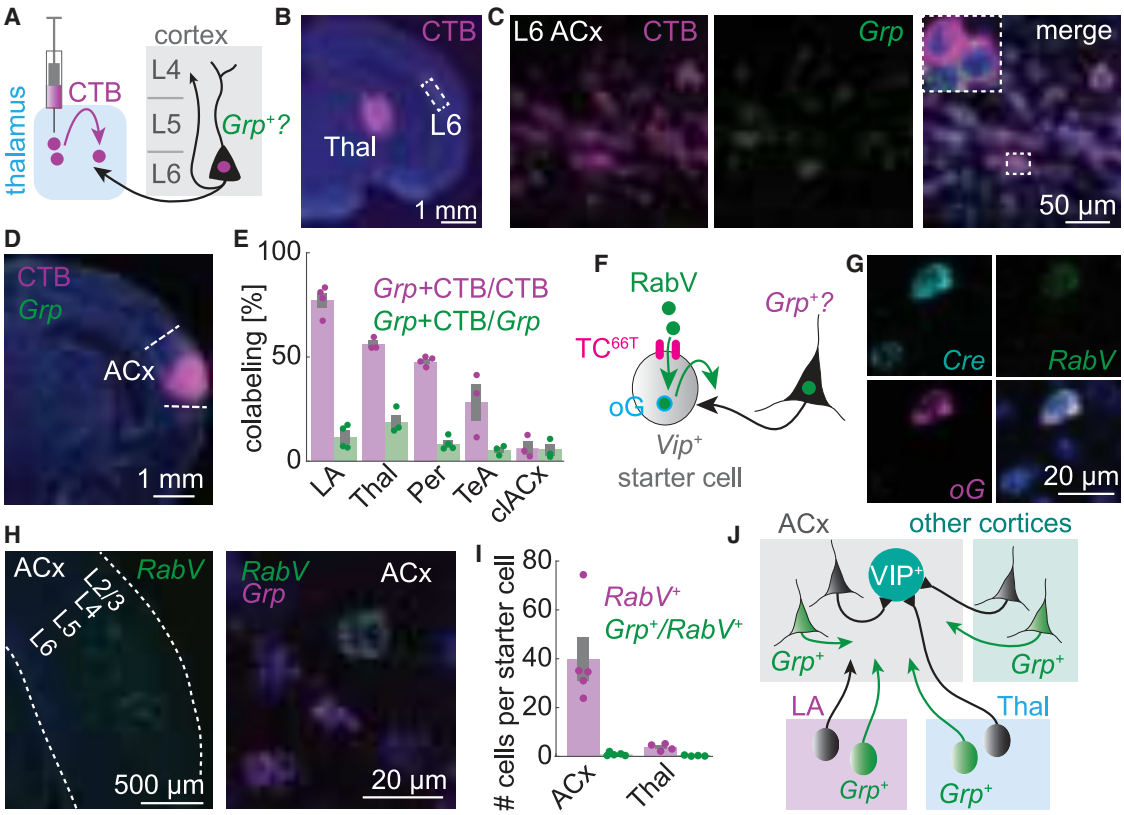

Figure 2. Putative local and long-range sources of GRP

(A) Schematic of retrograde tracing with CTB to quantify *Grp* expression in L6 cortico-thalamic neurons.

(B) Representative epifluorescent image of CTB injection into auditory thalamus (Thal) and retrograde labeling in auditory cortex (ACx) L6.

(C) Confocal image of retrogradely labeled cells in L6 of ACx and FISH against *Grp*. Inset: magnification of the highlighted area.

(D) Retrograde tracing with CTB injected into ACx to quantify *Grp* expression in corticopetal projection neurons. Epifluorescent image of a representative injection and FISH against *Grp*.

(E) Quantification of Grp^+ and CTB^+ cells in the indicated areas following injection as in (D). Each dot represents data from one mouse. Mean ± SEM across 358–1,142 CTB^+ cells per area. Abbreviations: LA, lateral amygdala; Per, perirhinal cortex; TeA, temporal association area; clACx, contralateral ACx.

(F) Schematic of transsynaptic tracing from Vip^+ starter cells using pseudotyped rabies virus SADΔG-EnVA-H2B-EGFP (RabV).

(G) Confocal image of an exemplary Vip^{Cre+} starter cell in ACx identified by *RabV-gp1* (RabV), *oG* and *Cre* (FISH).

(H) Confocal images of *RabV-gp1*$^+$ cells in ACx (left) and of an exemplary Grp^+/*RabV-gp1*$^+$ cell (right).

(I) Quantification of numbers of *RabV-gp1*$^+$ and Grp^+ cells after injections into ACx normalized to the numbers of starter cells. Each dot represents data from one mouse. Mean ± SEM.

(J) Schematic of putative Grp^+ inputs to ACx VIP cells.

See also Figure S2.

difference was found between PVALB cell depolarizations upon GRP application and in control recordings without GRP (Figure S3D), confirming that VIP cells are the preferential target of GRP.

The GRP-evoked subthreshold depolarization of most VIP cells in cortex suggests that GRPR signaling increases excitability in these cells. Indeed, GRP bath application significantly increased the evoked spike probability of VIP cells in response to optogenetic stimulation of thalamo-cortical afferents without increasing spontaneous spike rate prior to stimulation onset (Figure S3H).

Previous reports suggested that GRPR is a $G\alpha_q$-coupled receptor (Hellmich et al., 1997). A common secondary messenger of $G\alpha_q$ signaling is intracellular calcium (Ca^{2+}). To visualize Ca^{2+} dynamics and facilitate the identification of VIP cells in acute slices, we coexpressed the large-stokes shift red fluorophore mBeRFP (Yang et al., 2013) stoichiometrically with GCaMP using a self-cleaving P2A peptide linker (Figure 3F). Bath application of GRP increased GCaMP fluorescence in most VIP cells in ACx of male and female mice and in M1 at concentrations as low as 3 nM (Figures 3G, 3H, S3I, and S3J). Reminiscent of the GRP-induced burst activity in some VIP cells (Figures 3B and S3E), GCaMP fluorescence exhibited non-synchronized phasic (oscillatory) fluctuations at various frequencies in 26% of imaged VIP cells (Figures 3H, 3I, and S3K) that were partially blocked by TTX (14% of cells with Ca^{2+} oscillations) (Figures 3I, S3L, and S3M), suggesting that the majority of GRP-induced Ca^{2+}

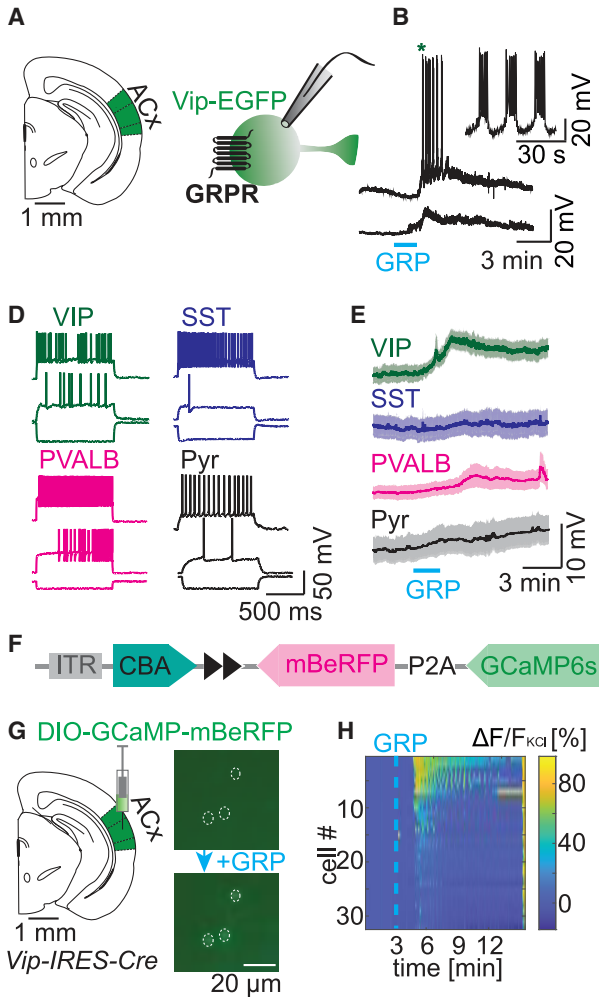

Figure 3. GRP depolarizes and increases intracellular Ca^{2+} in cortical VIP cells

(A) Schematic of whole-cell recording of ACx VIP cell used to examine effects of GRP.

(B) Two exemplary VIP cells responding with bursts (top) or depolarization (bottom) following 2-min bath application of GRP (300 nM) in the presence of NBQX, CPP, gabazine, and CGP. Inset: magnification of first bursts indicated by an asterisk.

(C) Depolarization of VIP cells upon application of indicated concentrations of GRP. Mean ± SEM, n = 6–10 cells per group. Comparison 0 versus 300 nM GRP: t test for unequal variance: t(12.52) = 3.76, p = 0.01. Other comparisons not significant (n.s.). Bath contains NBQX, CPP, gabazine, and CGP.

(D) Representative firing patterns of ACx VIP, SST, PVALB, and pyramidal (Pyr) cells upon −200 pA current injection (bottom), at AP threshold (middle), and at maximal firing rate (top).

(E) Average time course (left) and amplitude (right) of the membrane potential changes in each indicated cell type in ACx following GRP application. Bath contains NBQX, CPP, gabazine, CGP, and TTX. Mean ± SEM, n = 10 VIP, SST, Pyr cells, and 15 PVALB cells. Comparison to VIP cells (Bonferroni-corrected t test): SST: t(18) = −5.27, p < 0.001; PVALB: t(23) = −3.83, p < 0.001; Pyr: t(18) = −4.87, p < 0.001.

(F) Design of plasmid for Cre-dependent stoichiometric expression of GCaMP and mBeRFP for imaging of Ca^{2+} entry and detection of infected cells, respectively.

(G) Injection of AAV DIO-GCaMP-P2A-mBeRFP into ACx of male Vip^{Cre} mice (left) and epifluorescent GCaMP imaging (right) in acute slices before (top) and after (bottom) GRP bath application, in the presence of NBQX, CPP, gabazine, and CGP.

(H) Heatmap of fluorescence changes (expressed relative to fluorescence following KCl application, $\Delta F/F_{KCl}$) across all imaged VIP cells in an exemplary acute ACx slice.

(I) GCaMP fluorescence changes with or without TTX in two exemplary VIP cells (top) or across all recorded cells (bottom) in the presence of NBQX, CPP, gabazine, and CGP. Mean ± SEM, Mann-Whitney U test: U = 10178, p < 0.0001. n = 218 (−TTX) and 179 (+TTX) cells in 7 and 6 slices, respectively.

See also Figure S3.

signaling is AP-dependent. The AP-independent Ca^{2+} elevations are consistent with regulation of intracellular Ca^{2+} release from internal stores by $G\alpha_q$- and IP_3-mediated signaling. The delay between GRP application and changes in intracellular Ca^{2+} were largely due to delays in the infusion system (Figure S3N). In summary, our data indicate that GRP is a selective modulator of VIP cell signaling. Unfortunately, grpLight is not able to detect functionally relevant GRP levels *in vivo* as analysis of intracellular Ca^{2+} in VIP cells shows that GRP infusion has functional effects on these cells *in vivo* well before photometric detection of changes in grpLight fluorescence (Figure S3O).

GRP disinhibits cortex and induces IEG expression

The main circuit effect of VIP cell activation in the cortex is inhibition of SST and PVALB cells (Karnani et al., 2016; Pi et al., 2013) (Figure 4A). To test whether GRP leads to similar network effects, we recorded inhibitory postsynaptic currents (IPSCs) in SST and PVALB cells in acute ACx slices (Figures 4B and 4C). Bath application of GRP increased IPSC frequencies in 60% of SST and 40% of PVALB cells in a TTX-sensitive manner. IPSC frequencies increased only in 1 out of 10 Pyr cells, consistent with sporadic direct inhibition of Pyr cells by VIP cells (Chiu et al., 2018). Similar effects were observed in M1 (Figures S4A and S4B). EPSC frequency was hardly affected (Figure S4C), suggesting that inhibition of SST cells is the main direct network effect of GRP-mediated VIP cell activation.

Because VIP cell-mediated disinhibition of Pyr cells strongly depends on the activity level of SST cells, we examined GRP-mediated disinhibition of Pyr cells *in vivo*. To this end, we injected GRP into M1 of anaesthetized mice and used expression of the IEG *Fos* as an indicator of neuronal activity (Sheng et al., 1990). We revealed a strong increase in Fos (*Fos*) expression ipsilateral

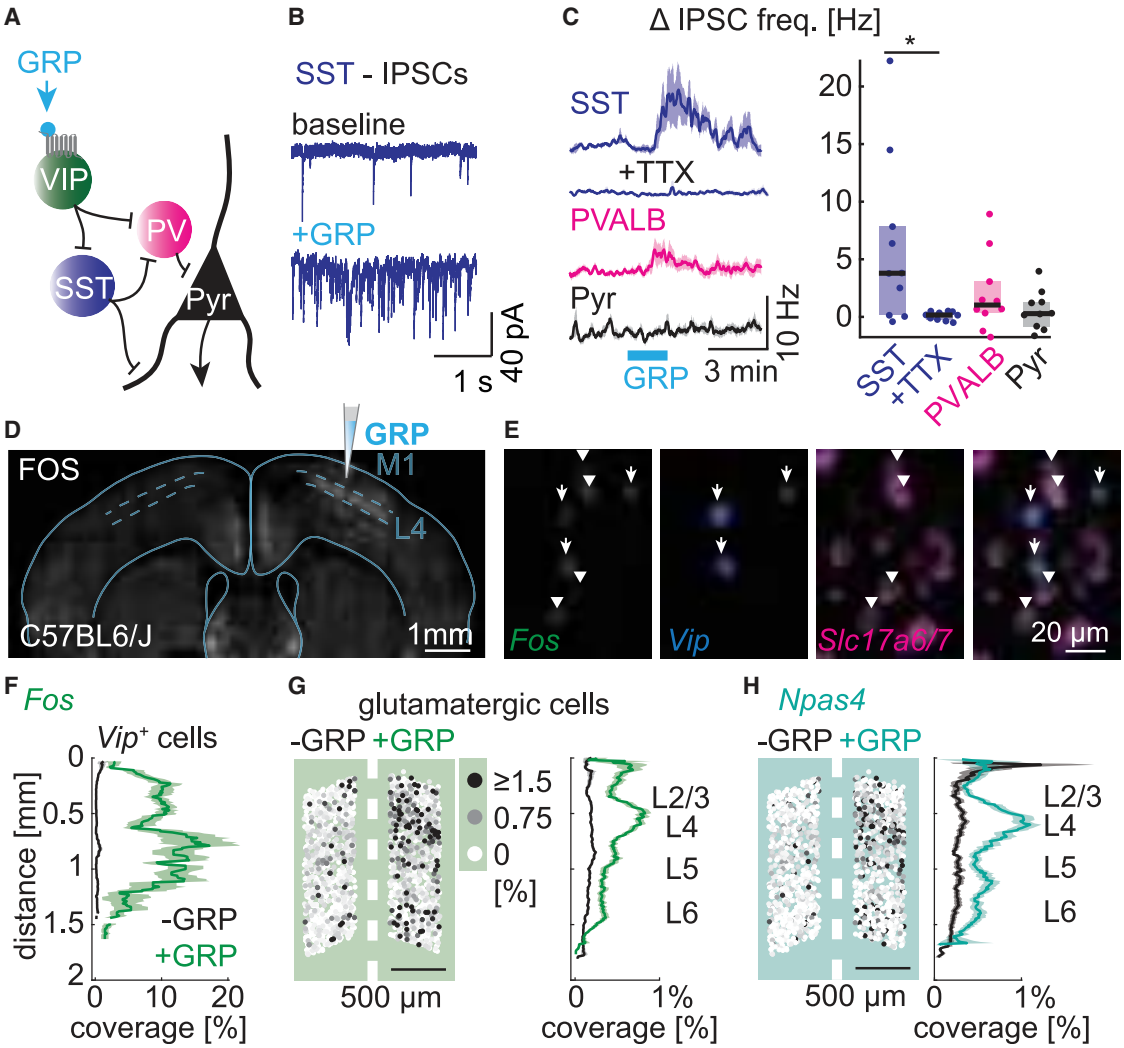

Figure 4. GRP disinhibits cortex and induces IEG expression

(A) Schematic of the disinhibitory circuit that underlies VIP cell function in cortex.

(B) Whole-cell recordings of IPSCs in a representative SST cell in ACx before (top) and following (bottom) GRP application in the presence of NBQX and CPP.

(C) Time courses (left, mean ± SEM) and magnitude (right, median and IQR) of IPSC frequency changes in SST, PVALB and Pyr cells (n = 10 cells per group) in the presence of NBQX and CPP (TTX where indicated). Mann-Whitney U test: U = 21, p = 0.03.

(D) Representative epifluorescent image of FOS immunostaining after injection of 3 µM GRP, as schematized, into the right motor cortex in anaesthetized mice.

(E) Confocal images of *Fos* expression in *Vip*$^+$ (arrows) and glutamatergic cells (arrowheads) analyzed using FISH.

(F–H) *Fos* and *Npas4* expression levels in *Vip*$^+$ and glutamatergic cells across all cortical layers for the right (green/turquoise) and left (black) motor cortices (mean ± SEM). Intensity-coded map of expression levels (% coverage) of all glutamatergic cells in an exemplary slice shown on the left (G and H). n = 398 (*Vip*), 15,108 (*Slc17a6,7*) cells, 3–5 mice for each condition and cell type.

See also Figure S4.

to the injection site (Figures 4D and S4D) in *Vip*$^+$ and glutamatergic cells across most cortical layers, without changes in expression in *Sst*$^+$ and *Pvalb*$^+$ cells (Figures 4E–4G, S4D1, and S4D2). Importantly, GRP injections into M1 of mice lacking GRPR specifically in VIP cells (*Vip-IRES-Cre;Grpr*$^{fl/y}$) (Yu et al., 2017) (Figures S4E1 and S4E2) or injections of the diluent (NRR) alone (Figures S4F1 and S4F2) led to significantly smaller increases in *Fos* expression (Figure S4G). A previous study indicated that *Fos* expression can be induced by a broad range of neuromodulatory inputs, whereas expression of another IEG, *Npas4*, is more tightly regulated by neuronal activity (Lin et al., 2008). We found that GRP injections lead to similar changes in *Npas4* levels, with significantly increased expression in *Vip*$^+$ and glutamatergic cells, but not *Sst*$^+$ and *Pvalb*$^+$ cells (Figures 4H and S4D3). *Npas4* expression was significantly smaller when GRP was injected into *Vip-IRES-Cre;Grpr*$^{fl/y}$ mice (Figures S4E3–S4G), confirming GRP-mediated disinhibition of glutamatergic cells through VIP cell-specific GRPR signaling.

ACx VIP cell activity encodes novel sounds and shocks during fear conditioning

The presence of *Grp*$^{+}$ cortically projecting neurons in all areas of the thalamo-cortico-amygdala loop, a circuit central for the encoding of fear memories (Boatman and Kim, 2006), together with previous reports of stress- and fear-induced GRP release in the amygdala (Merali et al., 1998; Mountney et al., 2011) suggest that GRP modulates sensory processing in cortex in the presence of aversive cues. An ideal behavioral paradigm to examine this possibility is auditory discriminatory fear conditioning (Dalmay et al., 2019; Letzkus et al., 2011). Unlike many tasks that depend on simple sounds, memory in this task requires activity in ACx and is modulated by disinhibitory circuits (Dalmay et al., 2019; Letzkus et al., 2011).

To determine whether VIP cells in the ACx are recruited during this task, we recorded bulk Ca^{2+}-dependent fluorescence changes using fiber photometry. To optimize comparison of VIP cell activity across mice and behavioral sessions, we tested the suitability of the GCaMP6s-P2A-mBeRFP construct for quantitative analysis of GCaMP fluorescence *in vivo*. Characterization of emission spectrum, Ca^{2+}-sensitivity, and relative expression levels, as well as physiological properties of VIP cells expressing GCaMP-P2A-mBeRFP (Figures 5A–5G and S5A–S5E) confirmed that mBeRFP can be used as a reference to normalize GCaMP fluorescence and to detect movement artifacts and patchcord detachment or entanglement.

We acquired fiber-photometric recordings in GCaMP6s-P2A-mBeRFP-expressing VIP cells in the right ACx during fear conditioning (Figures 5H and S5F–S5I). We observed strong fluorescence increases in VIP cells in response to novel conditioned (CS^{+}) and unconditioned (CS^{-}) sounds and foot shocks (Figure 5H). The responses were not due to movement artifacts as demonstrated by stable mBeRFP fluorescence (Figure S5J). The strong initial activation upon foot shocks, which triggered fast escape behavior, raises the possibility that VIP cell activity may be correlated with locomotion. However, neither the trial-averaged fluorescence during movement initiation after bouts of freezing nor cross-correlation of GCaMP fluorescence and speed revealed strong GCaMP modulation by locomotion (Figures S5K and S5L).

To test how GRP modulates the VIP cell dynamics *in vivo*, we compared GCaMP fluorescence in response to novel sounds and shocks before and after local infusion of GRP via a cannula. GRP increased peak responses of VIP cells to sounds and shocks without increasing discriminability between different stimuli (Figures 5I and S5M), suggesting a function in cortical state modulation rather than stimulus-specific encoding.

GRPR signaling in the ACx enhances fear memories

To test whether GRP/GRPR signaling contributes to the modulation of fear memories, we used CRISPR-Cas9-mediated KO of *Grpr* (Figure 6A). The efficiency of *Grpr* KO was confirmed by Ca^{2+} imaging in ACx VIP cells (Figures 6B and S6A). Bilateral AAV-mediated CRISPR-Cas9 injections into the ACx of male wild-type mice resulted in SaCas9-HA expression mainly in ACx (Figures 6C, S6B, and S6C). Electrophysiological analysis of ACx VIP cells did not reveal any significant changes in basic physiological parameters (Figures S6D and S6E), suggesting that VIP cells are healthy and do not develop intrinsic compensatory mechanisms when GRPR is ablated. Fear conditioning of ctrl and KO mice increased freezing during CS^{+} and CS^{-} throughout the conditioning session in both groups (Figure 6D). 24 hr after conditioning, mice were subjected to auditory fear memory retrieval. Freezing levels during CS^{+} and CS^{-} were significantly reduced in KO mice compared to ctrl mice (Figures 6E, 6F, and S6F), indicating a function of GRPR signaling in enhancing cortex-dependent memory formation.

Neither the absolute freezing difference between CS^{+} and CS^{-} (2-sample t test: $t[28] = 1.59$, $p = 0.12$) nor the discrimination index (STAR Methods) were significantly different in ctrl and KO mice (Figure 6G), indicating that the behavioral effect is not due to an impairment in auditory discrimination. Because freezing levels did not change significantly over time, and freezing levels in KO mice were strongly reduced even during the first 4 CS^{+} and CS^{-} (Figures S6G and S6H), we conclude that the reduced freezing in KO mice is not due to accelerated fear extinction. Moreover, reduced freezing levels in KO mice were not purely a result of increased baseline freezing, since freezing levels were still significantly reduced in KO mice after subtraction of baseline freezing (Figure S6I).

Importantly, ctrl and KO mice exhibited comparable locomotion during the conditioning session at baseline, during the first sounds and in response to the first foot shock (Figures S6J and S6K), indicating that the reduced freezing level in KO mice was not a result of different pain sensitivity or overall activity levels.

To verify that the behavioral effects were due to GRP-GRPR signaling and not ligand-independent recruitment of GRPR signaling, we injected CRISPR-Cas9 constructs into *Grp*$^{-/-}$ KO mice and subjected mice to the same behavioral testing paradigm. Freezing levels during CS^{+} and CS^{-} were not significantly different in *Grp*$^{-/-}$ mice injected with CRISPR-Cas9 constructs targeting *Grpr* or ctrl sequences (Figures 6H, S6L, and S6M), indicating that GRP signaling is required for the behavioral effects of GRPR. Importantly, *Grpr-Vip* coexpression was maintained in *Grp*$^{-/-}$ KO mice (Figure S6N), confirming that the absence of behavioral effects was not due to a lack of GRPR expression in VIP cells of *Grp*$^{-/-}$ KO mice.

To further exclude that the observed behavioral effects were due to side effects, we repeated the behavioral experiments using conditional *Grpr* KO mice (Yu et al., 2017). We validated Cre-dependent KO of *Grpr* in these mice using Ca^{2+} imaging (Figure 7A). To KO *Grpr* specifically in the ACx, we injected AAV hSyn-Cre-mCherry bilaterally into the ACx of *Grpr*$^{fl/y}$ (KO) or *Grpr*$^{wt/y}$ (ctrl) mice (Figures 7B and S7A). Four weeks after injection, both groups of mice were exposed to fear conditioning and retrieval as above. Freezing levels in KO mice upon presentation of CS^{+} and CS^{-} during retrieval were significantly reduced, with no significant effect on auditory discrimination (Figures 7C, 7D, S7B, and S7C). Importantly, the reduced freezing levels in KO mice were not caused by differences in genetic background of *Grpr*$^{fl/y}$ and *Grpr*$^{wt/y}$ mice because freezing levels in uninjected *Grpr*$^{fl/y}$ mice were not different from their ctrl littermates (Figures S7D and S7E), confirming that *Grpr* KO in the ACx reduces fear-induced freezing in a discriminatory auditory fear conditioning paradigm.

To examine the functional and context-dependent implications of GRP-GRPR signaling for VIP cells *in vivo*, we quantified

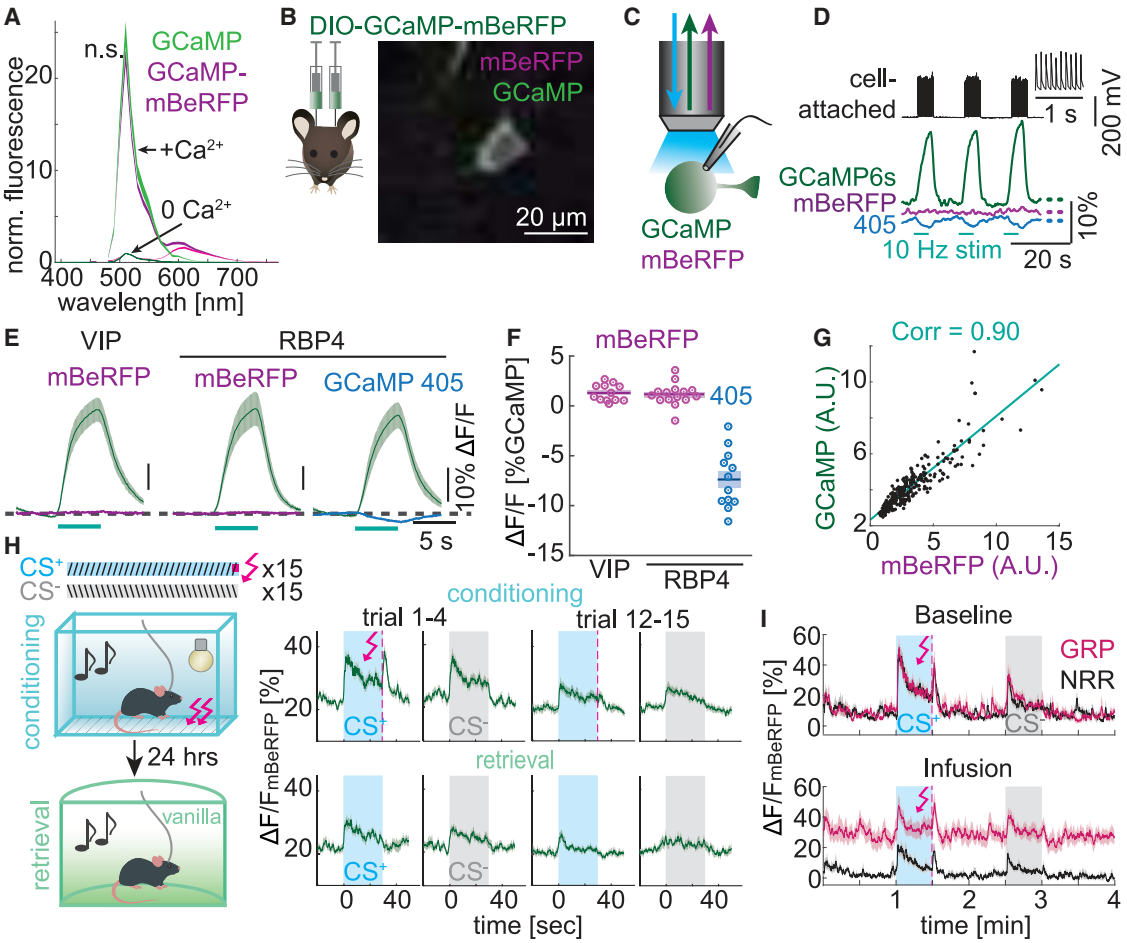

Figure 5. ACx VIP cells encode novel sounds and shocks during fear conditioning

(A) Fluorescence emission spectrum of GCaMP alone (green) and GCaMP-P2A-mBeRFP (magenta, pink) expressed in HEK293T cells and measured with or without application of Ca^{2+}/ionomycin, indicating that mBeRFP does not interfere with GCaMP6s fluorescence. 2-sample t test: $t(10) = -0.12$, $p = 0.91$; $n = 6$ wells each.

(B) Confocal image of a Pyr cell after injection of AAV DIO-GCaMP-P2A-mBeRFP and AAV Cre into ACx.

(C) Schematic of experimental setup for analysis of AP-dependent changes of GCaMP and mBeRFP fluorescence in acute brain slices during electrophysiological induction of spiking in VIP or L5 Pyr cells expressing GCaMP-P2A-mBeRFP in ACx of *Vip-IRES-Cre* and Rbp4-Cre mice.

(D) AP bursts (each 5-s at 10 Hz) induced in an exemplary $RBP4^+$ neuron through a cell-attached electrode (top) with GCaMP and mBeRFP fluorescence (473 nm excitation, middle) and GCaMP fluorescence (405 nm excitation, bottom). Inset: individual spikes from the last burst.

(E) Average GCaMP and mBeRFP (473 nm excitation) and GCaMP (405 nm excitation) fluorescence changes (ΔF/F). Data from cell-attached and whole-cell recordings were pooled. Dashed line: baseline fluorescence. Mean ± SEM from $n \geq 3$ mice each; n = 12 VIP, 15 RBP4 GCAMP/mBeRFP, and 12 RBP4 GCaMP (405 nm) cells.

(F) Quantification of fluorescence changes shown in (E) normalized to GCaMP (473 nm) fluorescence change. mBeRFP fluorescence was largely unaffected by neuronal activity. In comparison, GCaMP fluorescence was reduced when excited at 405 nm (−7.4% ± 0.8%).

(G) Correlation of GCaMP and mBeRFP fluorescence in Vip^+ cells after injection of AAV DIO-GCaMP-P2A-mBeRFP into ACx of *Vip-IRES-Cre* mice (linear regression and correlation coefficient in cyan). n = 335 cells from 3 injection sites.

(H) GCaMP fluorescence changes measured in ACx VIP cells around presentation of conditioned (CS^+, blue) and unconditioned sounds (CS^-, gray) and shocks (dashed pink lines) early (trials 1–4) and late (trials 12–15) on the conditioning (top) or retrieval (bottom) day. n = 11 mice.

(I) GCaMP fluorescence changes measured around presentation of CS^+ (blue) and CS^- (gray) and shocks (dashed pink lines) before (top) and following (bottom) infusion of GRP (pink) or control solution (NRR, black). n = 8 (GRP) and 7 (NRR) mice.

Data in (A) and (F)–(I): mean ± SEM.

See also Figure S5.

Fos expression in ACx Vip^+ cells three weeks after AAV-mediated injections of CRISPR-Cas9 constructs into the ACx of wild-type mice. *Fos* expression in Vip^+ cells lacking GRPR was significantly lower than in ctrl cells directly after fear conditioning but not in naive mice (Figures S7F and S7G), consistent with context-dependent recruitment of endogenous GRPR signaling. In line with this finding, amygdalo-cortical and thalamo-cortical projection neurons, a majority of which expresses *Grp*

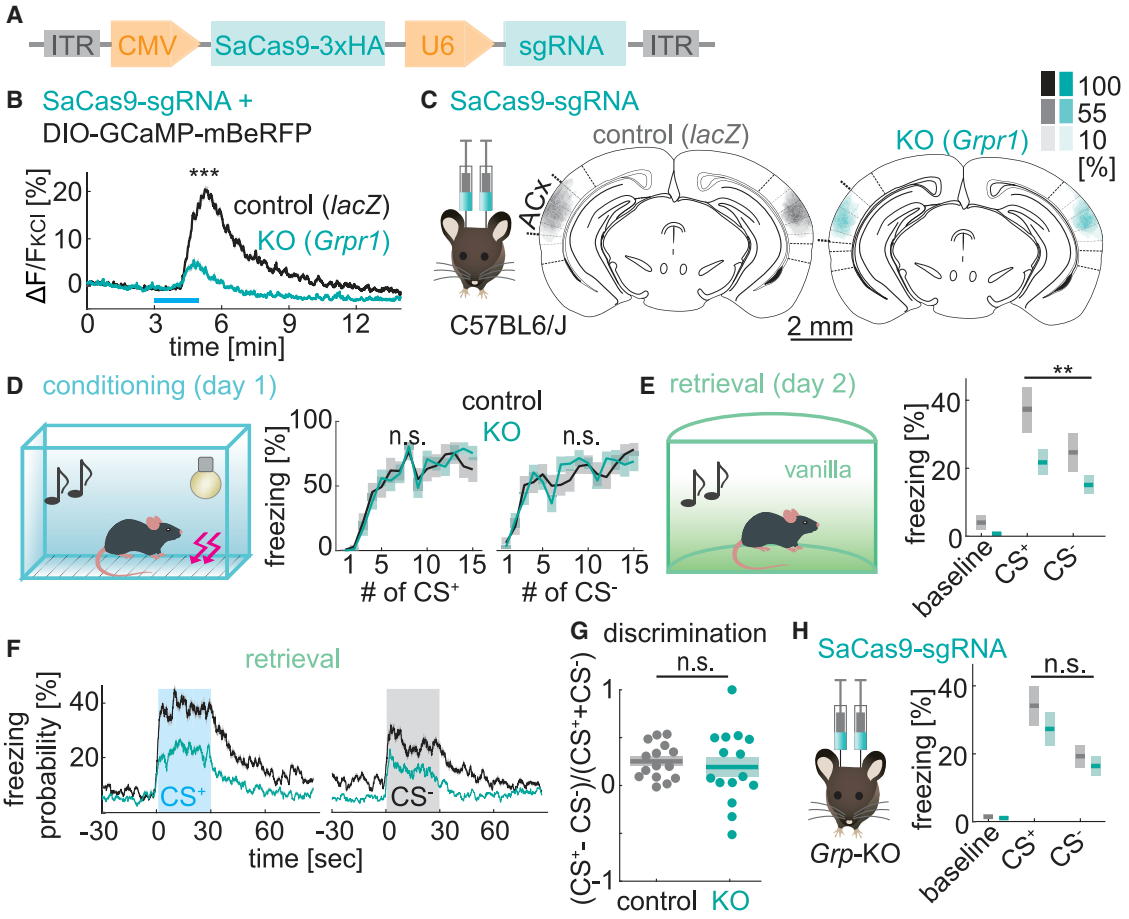

Figure 6. GRPR signaling in the ACx enhances fear memories

(A) Design of the plasmid for CRIPSR/Cas9-mediated KO of *Grpr* (abbreviated here as SaCas9-sgRNA) (Tervo et al., 2016).

(B) GCaMP fluorescence changes measured in acute slices upon GRP application for VIP cells expressing GCaMP-P2A-mBeRFP and SaCas9-sgRNA targeting either *Grpr* (KO, *Grpr1*) or *lacZ* (ctrl). Mann-Whitney U test: U = 25,956; $p < 0.0001$; n = 602 and 298 cells in 10 (ctrl) and 9 (KO) slices.

(C) Quantification of bilateral SaCas9-HA expression after injection of SaCas9-sgRNA targeting *lacZ* (ctrl, gray) or *Grpr* (KO, turquoise). See Figure S6 for analysis of expression in the whole brain. Color code: % of mice with SaCas9-HA expression.

(D) Auditory fear acquisition, measured as the percentage of time spent freezing during presentation of 15 CS^+ and CS^- on conditioning day (histology shown in C). 2-way ANOVA, main effect of genotypes: CS^+: $p = 0.90$, $F = 0.01$; CS^-: $p = 0.78$, $F = 0.08$, no significant interaction of genotype and stimulus number. n = 15 mice per group.

(E) Auditory fear memory retrieval, measured as the percentage of time spent freezing averaged across 15 presentations of CS^+ and CS^- on the retrieval day. 2-way ANOVA: main effect of genotype: $p = 0.01$, $F = 6.41$, no significant interaction of genotype and stimulus (CS^+ versus CS^-).

(F) Time courses of average freezing probability across all CS^+ and CS^- during fear memory retrieval.

(G) Sound discrimination indices measured during retrieval. t test for unequal variance: $t(20.13) = 0.53$, $p = 0.60$.

(H) Auditory fear memory retrieval in CRISPR-Cas9-expressing $Grp^{-/-}$ KO mice, measured as the percentage of time spent freezing averaged across 15 presentations of CS^+ and CS^- on the retrieval day. 2-way ANOVA: main effect of genotype: $p = 0.28$, $F = 1.21$, no significant interaction of genotype and stimulus (CS^+ versus CS^-), n = 14 mice per group.

All summary data in (B) and (D–H) shown as mean ± SEM.

See also Figure S6.

(Figure 2E), activated reliably during shocks (and during sounds in the case of thalamic projections) (Figures 7E, 7F, S7H, and S7I) consistent with context-dependent activation of GRP^+ neurons.

DISCUSSION

GRPergic signaling for cortex-wide communication

Neuropeptidergic signaling has been suggested to interconnect cortical neurons and provide control over cortical homeostasis and plasticity (Smith et al., 2019). This hypothesis is supported by the cellular specificity of receptor-ligand expression patterns but has largely not been tested functionally. Here, we provide direct evidence that distinct peptidergic cell-to-cell communication channels, consistent with those predicted by mRNA expression patterns, exist and regulate cortex-dependent behaviors. Unlike synaptic communication channels that have the ability to modulate individual cells through point-to-point communication, our data support that GRP acts on a larger scale through

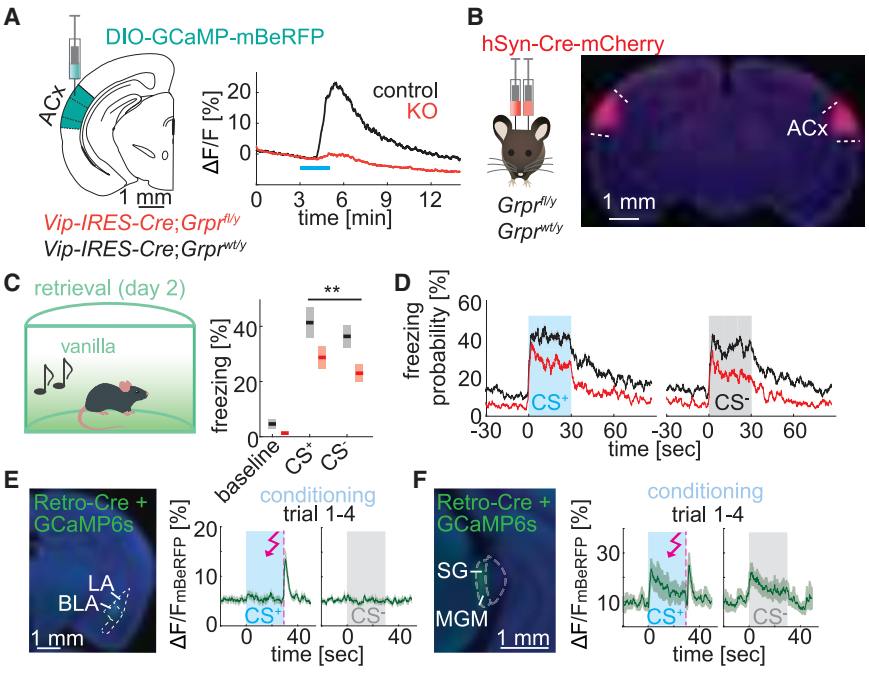

Figure 7. Impaired fear memory in mice with conditional KO of GRPR in the ACx

(A) GCaMP fluorescence changes in VIP cells following GRP application in acute ACx slices from ctrl mice (*Vip-IRES-Cre;Grpr*$^{wt/y}$) or mice lacking GRPR in VIP cells (*Vip-IRES-Cre;Grpr*$^{fl/y}$). Two-sample t test: t(1178) = 26.97, p < 0.0001, n = 655 cells in 14 slices (ctrl) and 525 cells in 11 slices (KO).

(B) Injection of AAV hSyn-Cre-mCherry into ACx of *Grpr*$^{wt/y}$ or *Grpr*$^{fl/y}$ mice to locally KO *Grpr*. Right: epifluorescent image of exemplary injection sites. Quantification of expression levels across all mice: Figure S7.

(C) Time spent freezing during fear memory retrieval in *Grpr*$^{wt/y}$ (ctrl) and *Grpr*$^{fl/y}$ (KO) mice injected into ACx with AAV encoding Cre-mCherry. 2-way ANOVA: main effect of genotype: p = 0.004, F = 8.99, no significant interaction of genotype and stimulus (CS^+ versus CS^-). n = 14 mice per group.

(D) Time course of average freezing probability across all CS^+ and CS^- presentations during fear memory retrieval.

(E) Photometric recordings from LA/BLA projection neurons, retrogradely tagged with AAVretro-Cre injections into the ACx. GCaMP fluorescence changes measured during CS^+ (blue), CS^- (gray), and shocks (dashed pink lines) during early conditioning trials (trials 1–4). n = 10 mice.

(F) Photometric recordings from thalamic SG/MGM projection neurons, retrogradely tagged with AAVretro-Cre injections into the ventral ACx and TeA. GCaMP fluorescence changes measured during early conditioning trials (trials 1–4). n = 5 mice.

All summary data in (A) and (C–F) shown as mean ± SEM.

See also Figure S7.

extrasynaptic diffusion (however, see "Limitations of study" below). This mode of transmission for neuropeptides was proposed several decades ago (Agnati et al., 1986) and is thought to be a major communication mode for neuromodulators (Taber and Hurley, 2014).

Cortical GRPR signaling enhances fear memories

Neuromodulators are thought to mediate context-dependent control over functional cortical circuits (Marlin et al., 2015; Nakajima et al., 2014; Polack et al., 2013; Smith et al., 2019). Here, we provide evidence for a previously unknown peptidergic control mechanism of behaviorally-relevant cortical circuits. Our data suggest that GRP is released in a context-dependent manner to increase plasticity as needed to strengthen memories in the presence of aversive or threatening cues. Interestingly, although our tracing studies reveal that TeA receives strong direct synaptic drive from GRP^+ amygdala projection neurons, inputs to primary ACx are non-synaptic, suggesting two distinct modes of action in these brain areas. We predict that the non-synaptic mode supports slower and longer-lasting modulation through activation of neuromodulatory receptors like GRPR, whereas the fast synaptic inputs to the TeA support stimulus-specific information transfer. State- or context-dependent release of GRP in the primary ACx cortex is thus optimal to broadly increase responses to and plasticity evoked by environmental stimuli without altering stimulus discriminability. Our behavioral results showing impaired fear memory, but unchanged sound discrimination, support such a scenario.

VIP cells are recruited by novel sounds and shocks

Although it is generally accepted that VIP cells are important regulators of cortical disinhibition and plasticity (Fu et al., 2014, 2015; Karnani et al., 2016; Pfeffer et al., 2013; Pi et al., 2013), evidence for memory and learning enhancement by VIP cells is surprisingly scarce (Adler et al., 2019; Fu et al., 2015). VIP cell responses to sounds and aversive cues (air puffs) were observed previously in head-fixed animals (Pi et al., 2013), but it was unknown how VIP cells encode the changing valence of conditioned and unconditioned cues during fear conditioning. Interestingly, similar to amygdala VIP cells (Krabbe et al., 2019), we observed strong activation of VIP cells by unexpected shocks and habituation of VIP cell responses to shocks with learning of the sound-shock association. In contrast to amygdala VIP cells, however, we also observed strong responses to novel sounds, which later habituated, suggesting that the responses to unexpected sounds and shocks may facilitate association learning by releasing inhibition and thereby increasing plasticity in distal dendrites of glutamatergic neurons. Interestingly, a distinct type of disinhibitory neurons in L1 of the ACx also exhibits strong activation to shocks (Letzkus et al., 2011), suggesting that both cells act synergistically to disinhibit Pyr neurons (Letzkus et al., 2011). Furthermore, our data show that GRPR activation increases excitability of VIP cells *in vitro* and induction of IEG transcription *in vivo*. These data suggest that GRP-GRPR signaling leads to the observed memory enhancement by increasing non-discriminatory VIP cell responses, and thereby inducing plasticity in VIP cells that regulate disinhibition in a subset of glutamatergic neurons.

Toward a complete picture of neuromodulatory control of cortical circuits

The daunting task of unraveling the multitude of neuromodulatory effects on signal transmission and plasticity across all cortical cell types may be essential to understand how cortical function is modulated in different emotional/physiological states by the plethora of neuropeptide receptors (Smith et al., 2019; Tasic et al., 2016, 2018). The heterogeneity of expression patterns and the diversity of receptors per cell type (Smith et al., 2019; Tasic et al., 2016, 2018) offer a glimpse into how intricate and versatile neuromodulator effects in the cortex can be. Together with previous studies (Li et al., 2016a; Marlin et al., 2015; Nakajima et al., 2014), our work underlines the importance for future studies to investigate additional cell-type-specific neuromodulatory communication channels and their impact on network activity and behavior.

Limitations of study

Although our experiments support a non-synaptic mode of transmission for GRP, we cannot exclude that point-to-point synaptic signaling by GRP also occurs. Thus, although our rabies virus experiments suggest only rare synaptic connectivity between GRP and VIP cells, these negative results might arise due to low efficiency of *trans*-synaptic transfer of rabies viruses at GRPergic synapses. In addition, we were not able to identify when GRP is released to modulate fear memories. This reflects a general gap in our understanding of neuropeptide signaling that results from two technical limitations: (1) a lack of understanding of the activity patterns that efficiently drive peptide release; and (2) a lack of sensors with sufficient sensitivity to detect released peptide. Improved GRP sensors will be beneficial to identify detailed spatial and temporal release dynamics also under physiological conditions *in vivo*.

Our photometric recordings of VIP cells *in vivo* did not reveal significant changes following ablation of GRPR. However, the significantly reduced *Fos* expression in VIP cells lacking GRPR following fear conditioning suggests that more sensitive techniques, such as 2-photon Ca^{2+} imaging and opto-tagged extracellular recordings, might reveal how GRPR modulates VIP cell activity patterns *in vivo* and identify the network mechanisms through which GRP-induced VIP cell plasticity and activity modulate behavioral outcomes.

STAR★METHODS

Detailed methods are provided in the online version of this paper and include the following:

- KEY RESOURCES TABLE
- RESOURCE AVAILABILITY
  - Lead contact
  - Materials availability
  - Data and code availability
- EXPERIMENTAL MODEL AND SUBJECT DETAILS
- METHOD DETAILS
  - Plasmids
  - Immunohistochemistry
  - Primary antibodies
  - Fluorescent *in situ* hybridization
  - Stereotactic AAV injections
  - Retrograde tracer injection (CTB)
  - Rabies virus tracing
  - Optogenetic stimulation
  - Immediate early gene expression analysis
  - RNA sequencing analysis
  - Electrophysiological recordings
  - HEK293T live-cell imaging
  - GCaMP-mBeRFP acute slice imaging
  - TAMRA-GRP imaging
  - Sensor engineering and characterization
  - Cannula infusion
  - Fear conditioning
  - Photometry
- QUANTIFICATION AND STATISTICAL ANALYSIS

ACKNOWLEDGMENTS

We thank Byung Kook Lim for providing starting material for rabies virus production, Zhou-Feng Chen for providing $GRPR^{fl/y}$ mice, and the Genome Engineering and iPSC core at Washington University, Zhihong Zhang, and Liqun Luo for providing plasmids. We thank Ivo Spiegel and Michael Greenberg for sharing unpublished data, Maree Webster for providing human tissue, and the Neurobiology Imaging Center for consultation and instrument availability. This facility is supported by the Neural Imaging Center as part of a NINDS P30 Core Center grant (NS072030). We thank Dr. Barbara Caldarone for behavioral training via the Harvard NeuroDiscovery Center. We thank members of the Sabatini lab for feedback on the manuscript and Carolyn Marie Orduno Davis for assisting with grpLight *in vitro* characterization. The research was funded by NIH (R35NS105107 to B.L.S. and U01NS115579 to L.T. and B.L.S.), Q-FASTR, the Nancy Laurie Marks Foundation, Bertarelli Foundation, and postdoctoral fellowships from DFG, EMBO, the Ellen R. and Melvin J. Gordon Center for the Cure and Treatment of Paralysis, and the Alice and Joseph Brooks Fund.

AUTHOR CONTRIBUTIONS

Conceptualization, S.M. and B.L.S.; methodology, S.M., B.L.S., L.T., K.W.H., and M.H.; formal analysis, S.M., E.R.N., A.C.P., and L.T.; investigation, S.M., E.R.N., G.O.M., M.H., A.C.P., E.Q., B.R., and M.R.G.; resources, K.W.H. and J.L.; writing, S.M. and B.L.S.; visualization, S.M., E.R.N., L.T., and B.L.S.; supervision, S.M., B.L.S., and L.T.; funding acquisition, B.L.S., L.T., and S.M.

DECLARATION OF INTERESTS

L.T. and G.O.M. are co-founders of Seven Biosciences.

Received: October 23, 2020
Revised: July 12, 2021
Accepted: September 8, 2021
Published: October 4, 2021

REFERENCES

Adler, A., Zhao, R., Shin, M.E., Yasuda, R., and Gan, W.B. (2019). Somatostatin-expressing interneurons enable and maintain learning-dependent sequential activation of pyramidal neurons. Neuron *102*, 202–216.e7.

Agnati, L.F., Fuxe, K., Zoli, M., Ozini, I., Toffano, G., and Ferraguti, F. (1986). A correlation analysis of the regional distribution of central enkephalin and β-endorphin immunoreactive terminals and of opiate receptors in adult and old male rats. Evidence for the existence of two main types of communication in the central nervous system: the volume transmission and the wiring transmission. Acta Physiol. Scand. *128*, 201–207.

Batista-Brito, R., Vinck, M., Ferguson, K.A., Chang, J.T., Laubender, D., Lur, G., Mossner, J.M., Hernandez, V.G., Ramakrishnan, C., Deisseroth, K., et al. (2017). Developmental dysfunction of VIP interneurons impairs cortical circuits. Neuron *95*, 884–895.e9.

Boatman, J.A., and Kim, J.J. (2006). A thalamo-cortico-amygdala pathway mediates auditory fear conditioning in the intact brain. Eur. J. Neurosci. *24*, 894–900.

Briggs, F., and Usrey, W.M. (2011). Corticogeniculate feedback and visual processing in the primate. J. Physiol. *589*, 33–40.

Chattopadhyaya, B., Di Cristo, G., Higashiyama, H., Knott, G.W., Kuhlman, S.J., Welker, E., and Huang, Z.J. (2004). Experience and activity-dependent maturation of perisomatic GABAergic innervation in primary visual cortex during a postnatal critical period. J. Neurosci. *24*, 9598–9611.

Chen, T.W., Wardill, T.J., Sun, Y., Pulver, S.R., Renninger, S.L., Baohan, A., Schreiter, E.R., Kerr, R.A., Orger, M.B., Jayaraman, V., et al. (2013). Ultrasensitive fluorescent proteins for imaging neuronal activity. Nature *499*, 295–300.

Chiu, C.Q., Martenson, J.S., Yamazaki, M., Natsume, R., Sakimura, K., Tomita, S., Tavalin, S.J., and Higley, M.J. (2018). Input-Specific NMDAR-Dependent Potentiation of Dendritic GABAergic Inhibition. Neuron *97*, 368–377.e3.

Dalmay, T., Abs, E., Poorthuis, R.B., Hartung, J., Pu, D.L., Onasch, S., Lozano, Y.R., Signoret-Genest, J., Tovote, P., Gjorgjieva, J., and Letzkus, J.J. (2019). A Critical Role for Neocortical Processing of Threat Memory. Neuron *104*, 1180–1194.e7.

Fenno, L.E., Mattis, J., Ramakrishnan, C., Hyun, M., Lee, S.Y., He, M., Tucciarone, J., Selimbeyoglu, A., Berndt, A., Grosenick, L., et al. (2014). Targeting cells with single vectors using multiple-feature Boolean logic. Nat. Methods *11*, 763–772.

Fu, Y., Tucciarone, J.M., Espinosa, J.S., Sheng, N., Darcy, D.P., Nicoll, R.A., Huang, Z.J., and Stryker, M.P. (2014). A cortical circuit for gain control by behavioral state. Cell *156*, 1139–1152.

Fu, Y., Kaneko, M., Tang, Y., Alvarez-Buylla, A., and Stryker, M.P. (2015). A cortical disinhibitory circuit for enhancing adult plasticity. eLife *4*, e05558.

Gong, S., Zheng, C., Doughty, M.L., Losos, K., Didkovsky, N., Schambra, U.B., Nowak, N.J., Joyner, A., Leblanc, G., Hatten, M.E., and Heintz, N. (2003). A gene expression atlas of the central nervous system based on bacterial artificial chromosomes. Nature *425*, 917–925.

He, M., Tucciarone, J., Lee, S., Nigro, M.J., Kim, Y., Levine, J.M., Kelly, S.M., Krugikov, I., Wu, P., Chen, Y., et al. (2016). Strategies and Tools for Combinatorial Targeting of GABAergic Neurons in Mouse Cerebral Cortex. Neuron *91*, 1228–1243.

Hellmich, M.R., Battery, J.F., and Northup, J.K. (1997). Selective reconstitution of gastrin-releasing peptide receptor with Gαq. Proc. Natl. Acad. Sci. USA *94*, 751–756.

Hodge, R.D., Bakken, T.E., Miller, J.A., Smith, K.A., Barkan, E.R., Graybuck, L.T., Close, J.L., Long, B., Johansen, N., Penn, O., et al. (2019). Conserved cell types with divergent features in human versus mouse cortex. Nature *573*, 61–68.

Iurilli, G., Ghezzi, D., Olcese, U., Lassi, G., Nazzaro, C., Tonini, R., Tucci, V., Benfenati, F., and Medini, P. (2012). Sound-driven synaptic inhibition in primary visual cortex. Neuron *73*, 814–828.

Jékely, G., Melzer, S., Beets, I., Kadow, I.C.G., Koene, J., Haddad, S., and Holden-Dye, L. (2018). The long and the short of it - a perspective on peptidergic regulation of circuits and behaviour. J. Exp. Biol. *221*, jeb166710.

Karnani, M.M., Jackson, J., Ayzenshtat, I., Hamzehei Sichani, A., Manoocheri, K., Kim, S., and Yuste, R. (2016). Opening holes in the blanket of inhibition: Localized lateral disinhibition by vip interneurons. J. Neurosci. *36*, 3471–3480.

Kim, E.J., Jacobs, M.W., Ito-Cole, T., and Callaway, E.M. (2016). Improved monosynaptic neural circuit tracing using engineered rabies virus glycoproteins. Cell Rep. *15*, 692–699.

Krabbe, S., Paradiso, E., d'Aquin, S., Bitterman, Y., Courtin, J., Xu, C., Yonehara, K., Markovic, M., Müller, C., Eichlisberger, T., et al. (2019). Adaptive disinhibitory gating by VIP interneurons permits associative learning. Nat. Neurosci. *22*, 1834–1843.

Kroog, G.S., Jensen, R.T., and Battey, J.F. (1995). Mammalian bombesin receptors. Med. Res. Rev. *15*, 389–417.

Lam, A.J., St-Pierre, F., Gong, Y., Marshall, J.D., Cranfill, P.J., Baird, M.A., McKeown, M.R., Wiedenmann, J., Davidson, M.W., Schnitzer, M.J., et al. (2012). Improving FRET dynamic range with bright green and red fluorescent proteins. Nat. Methods *9*, 1005–1012.

Lee, S., Kruglikov, I., Huang, Z.J., Fishell, G., and Rudy, B. (2013). A disinhibitory circuit mediates motor integration in the somatosensory cortex. Nat. Neurosci. *16*, 1662–1670.

Leinweber, M., Ward, D.R., Sobczak, J.M., Attinger, A., and Keller, G.B. (2017). A sensorimotor circuit in mouse cortex for visual flow predictions. Neuron *95*, 1420–1432.e5.

Letzkus, J.J., Wolff, S.B.E., Meyer, E.M.M., Tovote, P., Courtin, J., Herry, C., and Lüthi, A. (2011). A disinhibitory microcircuit for associative fear learning in the auditory cortex. Nature *480*, 331–335.

Li, K., Nakajima, M., Ibañez-Tallon, I., and Heintz, N. (2016a). A cortical circuit for sexually dimorphic oxytocin-dependent anxiety behaviors. Cell *167*, 60–72.e11.

Li, P., Janczewski, W.A., Yackle, K., Kam, K., Pagliardini, S., Krasnow, M.A., and Feldman, J.L. (2016b). The peptidergic control circuit for sighing. Nature *530*, 293–297.

Lin, Y., Bloodgood, B.L., Hauser, J.L., Lapan, A.D., Koon, A.C., Kim, T.K., Hu, L.S., Malik, A.N., and Greenberg, M.E. (2008). Activity-dependent regulation of inhibitory synapse development by Npas4. Nature *455*, 1198–1204.

Mandelbaum, G., Taranda, J., Haynes, T.M., Hochbaum, D.R., Huang, K.W., Hyun, M., Umadevi Venkataraju, K., Straub, C., Wang, W., Robertson, K., et al. (2019). Distinct cortical-thalamic-striatal circuits through the parafascicular nucleus. Neuron *102*, 636–652.e7.

Marlin, B.J., Mitre, M., D'amour, J.A., Chao, M.V., and Froemke, R.C. (2015). Oxytocin enables maternal behaviour by balancing cortical inhibition. Nature *520*, 499–504.

Merali, Z., McIntosh, J., Kent, P., Michaud, D., and Anisman, H. (1998). Aversive and appetitive events evoke the release of corticotropin-releasing hormone and bombesin-like peptides at the central nucleus of the amygdala. J. Neurosci. *18*, 4758–4766.

Miyamichi, K., Shlomai-Fuchs, Y., Shu, M., Weissbourd, B.C., Luo, L., and Mizrahi, A. (2013). Dissecting local circuits: parvalbumin interneurons underlie broad feedback control of olfactory bulb output. Neuron *80*, 1232–1245.

Mountney, C., Sillberg, V., Kent, P., Anisman, H., and Merali, Z. (2006). The role of gastrin-releasing peptide on conditioned fear: differential cortical and amygdaloid responses in the rat. Psychopharmacology (Berl.) *189*, 287–296.

Mountney, C., Anisman, H., and Merali, Z. (2008). Effects of gastrin-releasing peptide agonist and antagonist administered to the basolateral nucleus of the amygdala on conditioned fear in the rat. Psychopharmacology (Berl.) *200*, 51–58.

Mountney, C., Anisman, H., and Merali, Z. (2011). In vivo levels of corticotropin-releasing hormone and gastrin-releasing peptide at the basolateral amygdala and medial prefrontal cortex in response to conditioned fear in the rat. Neuropharmacology *60*, 410–417.

Nakajima, M., Görlich, A., and Heintz, N. (2014). Oxytocin modulates female sociosexual behavior through a specific class of prefrontal cortical interneurons. Cell *159*, 295–305.

Oliva, A.A., Jr., Jiang, M., Lam, T., Smith, K.L., and Swann, J.W. (2000). Novel hippocampal interneuronal subtypes identified using transgenic mice that express green fluorescent protein in GABAergic interneurons. J. Neurosci. *20*, 3354–3368.

Osakada, F., and Callaway, E.M. (2013). Design and generation of recombinant rabies virus vectors. Nat. Protoc. *8*, 1583–1601.

Owen, S.F., and Kreitzer, A.C. (2019). An open-source control system for in vivo fluorescence measurements from deep-brain structures. J. Neurosci. Methods *311*, 170–177.

Patriarchi, T., Cho, J.R., Merten, K., Howe, M.W., Marley, A., Xiong, W.H., Folk, R.W., Broussard, G.J., Liang, R., Jang, M.J., et al. (2018). Ultrafast neuronal

imaging of dopamine dynamics with designed genetically encoded sensors. Science *360*, eaat4422.

Pfeffer, C.K., Xue, M., He, M., Huang, Z.J., and Scanziani, M. (2013). Inhibition of inhibition in visual cortex: the logic of connections between molecularly distinct interneurons. Nat. Neurosci. *16*, 1068–1076.

Pi, H.J., Hangya, B., Kvitsiani, D., Sanders, J.I., Huang, Z.J., and Kepecs, A. (2013). Cortical interneurons that specialize in disinhibitory control. Nature *503*, 521–524.

Polack, P.O., Friedman, J., and Golshani, P. (2013). Cellular mechanisms of brain state-dependent gain modulation in visual cortex. Nat. Neurosci. *16*, 1331–1339.

Ran, F.A., Cong, L., Yan, W.X., Scott, D.A., Gootenberg, J.S., Kriz, A.J., Zetsche, B., Shalem, O., Wu, X., Makarova, K.S., et al. (2015). In vivo genome editing using Staphylococcus aureus Cas9. Nature *520*, 186–191.

Roesler, R., Meller, C.A., Kopschina, M.I., Souza, D.O., Henriques, J.A.P., and Schwartsmann, G. (2003). Intrahippocampal infusion of the bombesin/gastrin-releasing peptide antagonist RC-3095 impairs inhibitory avoidance retention. Peptides *24*, 1069–1074.

Rose, T., Jaepel, J., Hübener, M., and Bonhoeffer, T. (2016). Cell-specific restoration of stimulus preference after monocular deprivation in the visual cortex. Science *352*, 1319–1322.

Saunders, A., Johnson, C.A., and Sabatini, B.L. (2012). Novel recombinant adeno-associated viruses for Cre activated and inactivated transgene expression in neurons. Front. Neural Circuits *6*, 47.

Sheng, M., McFadden, G., and Greenberg, M.E. (1990). Membrane depolarization and calcium induce c-fos transcription via phosphorylation of transcription factor CREB. Neuron *4*, 571–582.

Smith, S.J., Sümbül, U., Graybuck, L.T., Collman, F., Seshamani, S., Gala, R., Gliko, O., Elabbady, L., Miller, J.A., Bakken, T.E., et al. (2019). Single-cell transcriptomic evidence for dense intracortical neuropeptide networks. eLife *8*, e47889.

Sun, Y.G., and Chen, Z.F. (2007). A gastrin-releasing peptide receptor mediates the itch sensation in the spinal cord. Nature *448*, 700–703.

Taber, K.H., and Hurley, R.A. (2014). Volume transmission in the brain: beyond the synapse. J. Neuropsychiatry Clin. Neurosci. *26*, 1–4.

Taniguchi, H., He, M., Wu, P., Kim, S., Paik, R., Sugino, K., Kvitsiani, D., Fu, Y., Lu, J., Lin, Y., et al. (2011). A resource of Cre driver lines for genetic targeting of GABAergic neurons in cerebral cortex. Neuron *71*, 995–1013.

Tasic, B., Menon, V., Nguyen, T.N., Kim, T.K., Jarsky, T., Yao, Z., Levi, B., Gray, L.T., Sorensen, S.A., Dolbeare, T., et al. (2016). Adult mouse cortical cell taxonomy revealed by single cell transcriptomics. Nat. Neurosci. *19*, 335–346.

Tasic, B., Yao, Z., Graybuck, L.T., Smith, K.A., Nguyen, T.N., Bertagnolli, D., Goldy, J., Garren, E., Economo, M.N., Viswanathan, S., et al. (2018). Shared and distinct transcriptomic cell types across neocortical areas. Nature *563*, 72–78.

Tervo, D.G.R., Hwang, B.Y., Viswanathan, S., Gaj, T., Lavzin, M., Ritola, K.D., Lindo, S., Michael, S., Kuleshova, E., Ojala, D., et al. (2016). A designer AAV variant permits efficient retrograde access to projection neurons. Neuron *92*, 372–382.

Tyan, L., Chamberland, S., Magnin, E., Camiré, O., Francavilla, R., David, L.S., Deisseroth, K., and Topolnik, L. (2014). Dendritic inhibition provided by interneuron-specific cells controls the firing rate and timing of the hippocampal feedback inhibitory circuitry. J. Neurosci. *34*, 4534–4547.

Wall, N.R., De La Parra, M., Sorokin, J.M., Taniguchi, H., Huang, Z.J., and Callaway, E.M. (2016). Brain-wide maps of synaptic input to cortical interneurons. J. Neurosci. *36*, 4000–4009.

Wickersham, I.R., Sullivan, H.A., and Seung, H.S. (2010). Production of glycoprotein-deleted rabies viruses for monosynaptic tracing and high-level gene expression in neurons. Nat. Protoc. *53*, 595–606.

Yang, J., Wang, L., Yang, F., Luo, H., Xu, L., Lu, J., Zeng, S., and Zhang, Z. (2013). mBeRFP, an improved large stokes shift red fluorescent protein. PLoS ONE *8*, e64849.

Yu, Y.Q., Barry, D.M., Hao, Y., Liu, X.T., and Chen, Z.F. (2017). Molecular and neural basis of contagious itch behavior in mice. Science *355*, 1072–1076.

Zhang, S., Xu, M., Kamigaki, T., Hoang Do, J.P., Chang, W.C., Jenvay, S., Miyamichi, K., Luo, L., and Dan, Y. (2014). Selective attention. Long-range and local circuits for top-down modulation of visual cortex processing. Science *345*, 660–665.

Zhao, Z.Q., Huo, F.Q., Jeffry, J., Hampton, L., Demehri, S., Kim, S., Liu, X.Y., Barry, D.M., Wan, L., Liu, Z.C., et al. (2013). Chronic itch development in sensory neurons requires BRAF signaling pathways. J. Clin. Invest. *123*, 4769–4780.